Journal of Hazardous Materials 265 (2014) 217–225

Contents lists available at ScienceDirect

Journal of Hazardous Materials

journal homepage: www.elsevier.com/locate/jhazmat

A novel approach for arsenic adsorbents regeneration using MgO

Sofia Tresintsi[a], Konstantinos Simeonidis[b], Maria Katsikini[c], Eleni C. Paloura[c], Georgios Bantsis[a], Manassis Mitrakas[a,*]

[a] Analytical Chemistry Laboratory, Department of Chemical Engineering, Aristotle University of Thessaloniki, 54124, Greece
[b] Department of Mechanical Engineering, University of Thessaly, 38334 Volos, Greece
[c] Department of Physics, Aristotle University of Thessaloniki, 54124, Greece

HIGHLIGHTS

- Low-cost and efficient regeneration of FeOOH arsenic adsorbents by MgO.
- Continuous flow NaOH recirculation system for on-site application in adsorption beds.
- As(V) is adsorbed onto MgO in the form of monodentate inner sphere complexes.
- Environmentally safe and profitable handling of saturated MgO in cement.

GRAPHICAL ABSTRACT

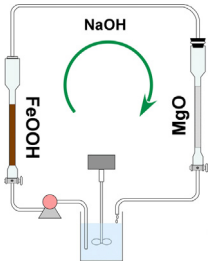

ARTICLE INFO

Article history:
Received 7 October 2013
Received in revised form
26 November 2013
Accepted 2 December 2013
Available online 7 December 2013

Keywords:
Magnesium oxide
Arsenic removal
Drinking water
Adsorbents regeneration
RSSCT
XAFS

ABSTRACT

An integrated procedure for the regeneration of iron oxy-hydroxide arsenic adsorbents by granulated MgO is proposed in this study. A continuous recirculation configuration, with a NaOH solution flowing sequentially through the saturated adsorbent (leaching step) and the MgO (adsorption step) column beds, was optimized by utilizing the high arsenic adsorption efficiency of MgO at strong alkaline environments. Experimental results indicated that the total amount of leached arsenic was captured by MgO whereas the regenerated iron oxy-hydroxide recovered around 80% of its removal capacity upon reuse. The improved adsorption capacity of MgO for As(V), which is maximized at pH 10, is explained by the intermediate hydration to $Mg(OH)_2$ and the following As(V) oxy-anions adsorption on its surface through the formation of monodentate inner sphere complexes, as it is deduced from the As—K-edge X-ray absorption fine structure (EXAFS) analysis. In addition to the economical-benefits, corresponding tests proved that the solid wastes of this process, namely spent $MgO/Mg(OH)_2$, can be environmentally safely disposed as stable additives in cement products, while the alkaline solution is completely detoxified and can be recycled to the regeneration task.

1. Introduction

Arsenic is considered as a toxic substance for human health, since it is implicated to various cancer types [1,2]. Thus, the presence of arsenic in drinking waters at concentrations higher than the maximum contaminant level of 10 μg/L resulted in the development of many removal methods such as chemical coagulation [3] and adsorption on activated alumina [4,5], activated carbon [6], iron oxy-hydroxides [7,8], TiO_2 [9–11], CeO_2 [12], ZrO_2 [13] and binary Fe/Mn structures [14]. Nevertheless, adsorption is nowadays the most commonly practiced method for arsenic removal, offering many advantages including simple and stable operation, easy handling of waste, absence of added reagents, compact facilities and acceptable operational cost [15]. Iron oxy-hydroxides (FeOOH) are the most widely used class of arsenic adsorbents, since they are able

* Corresponding author. Tel.: +30 2310 996248; fax: +30 2310 996248.
E-mail addresses: stresint@physics.auth.gr (S. Tresintsi), ksime@physics.auth.gr (K. Simeonidis), katsiki@auth.gr (M. Katsikini), paloura@auth.gr (E.C. Paloura), bantsis_george@yahoo.gr (G. Bantsis), manasis@eng.auth.gr, mmitraka@auth.gr (M. Mitrakas).

0304-3894/$ – see front matter © 2013 Elsevier B.V. All rights reserved.
http://dx.doi.org/10.1016/j.jhazmat.2013.12.003

to remove both arsenic species, As(III) and As(V), below the regulation limit at a high adsorption capacity, which is not influenced by the ionic strength and the interference of common inorganic ions of water. In addition to that, their affinity to arsenic is strong under natural pH conditions, resulting in irreversible arsenic adsorption whereas leaching tests verified that spent iron oxy-hydroxides are considered as inert [16,17].

However, the most significant disadvantage of the adsorption process is the high cost of the consumable adsorbents [17], and therefore, their possible regeneration could drastically decrease the total cost of water treatment. Usually, spent adsorbents can be regenerated by an alkaline solution (e.g. NaOH), which effectively leaches adsorbed arsenic [18]. The success of the regeneration process is signified by the recovery degree of adsorption capacity in the regenerated adsorbent compared to the fresh one. But the main issue of the process is the handling of the arsenic-rich regeneration solution. In some cases, arsenic is recovered from the regeneration solution as arsenic sulfide [19]. This process is rather complicated and increases the labor cost setting regeneration quite expensive. Thus, most arsenic adsorbents are preferably employed solely on a replacement (throw-away) basis.

Magnesium oxide (MgO), an alkaline earth metal oxide, is a low cost material with simple production process from abundant natural minerals. In the form of nanoparticles or nanowires, MgO has been recently reported to present high adsorption capacity for both As(III) and As(V) [20–22]. Although not clearly stated, the presented results in these studies, refer to equilibrium pH higher than 10, despite the fact that a neutral water pH was initially implemented. This comes out from the fact that MgO reacts with water to form $Mg(OH)_2$, which presents a strong alkaline character [23]. Therefore, arsenic adsorption/disposal by MgO implies adsorption/disposal by $MgO/Mg(OH)_2$. Magnesium hydroxide has high solubility in water at pH values below 9 [24] while it is practically insoluble at pH values above 10, as concluded from its solubility constant ($k_{sp} = 5.61 \times 10^{-12}$ at 25 °C). Therefore, MgO cannot be applied as arsenic adsorbent at the pH range of natural water, where it gets dissolved, but it is expected to function with high adsorption capacity at alkaline pH values, thus, reducing the arsenic concentration of a regeneration stream.

The motivation of this work is to establish an innovative continuous-flow procedure for on-site regeneration of iron oxy-hydroxides column beds, used for arsenic adsorption by taking the advantage of high arsenic capture efficiency of MgO at the alkaline environment of the regeneration stream. For this reason, the optimum conditions of MgO application and the arsenic adsorption mechanism were examined through batch adsorption tests. Following this information, a regeneration setup consisting of a saturated adsorbent and an MgO column was designed and monitored, simulating a large-scale system, in which a NaOH solution is continuously recirculated. Among the benefits of this configuration, which contributes to lower water treatment cost, are the reduction of the regeneration solution volume and its detoxification during the process. The study was integrated by investigation of the spent MgO effective stabilization in cement products as an environmental friendly, feasible and inexpensive approach for arsenic-containing MgO disposal.

2. Materials and methods

2.1. Adsorbents

A commercial fused-MgO (>98 wt%) was used in the form of fine powder (<63 μm) for batch adsorption tests and granulated material (100–250 μm) for regeneration column tests. This particular particle size for MgO was selected in order to comply with the specifications for spent MgO incorporation into concrete specimens. An iron oxy-hydroxide synthesized by $FeSO_4$ precipitation at pH 5.5 and high oxidizing environment as described in Ref. [25], was applied as a typical arsenic adsorbent to perform the saturation–regeneration cycle. Specific surface area of the materials was estimated by nitrogen gas adsorption at liquid N_2 temperature (77 K) using a micropore surface area analyzer according to the Brunauer–Emmett–Teller (BET) model. The isoelectric point (IEP) was determined by the curve of zeta-potential at 20 ± 1 °C, using a Rank Brothers Mk II micro-electrophoresis apparatus. Thermogravimetric analysis (TG-DTA) was performed on a water-cooled Perkin-Elmer STA 6000 instrument in the temperature range 50–900 °C, at a heating rate of 20 °C/min under nitrogen flow. Examination of materials morphology variation after treatment was performed using a Carl Zeiss EVO 50 XVP scanning electron microscope (SEM). The corresponding structural changes were studied by X-ray diffraction (XRD) using a Panalytical X'pert PRO diffractometer with CuK_α radiation.

2.2. Reagents

Stock solutions of As(III) and As(V) (1000 mg/L) were prepared by diluting proper amounts of $NaAsO_2$ and $Na_2HAsO_4{\cdot}7H_2O$, respectively, in distilled water. Working standards were prepared by proper dilution of the stock solutions. The pH values of all arsenic solutions were adjusted either by NaOH or HCl addition. The natural test water was prepared according to National Sanitation Foundation (NSF) standard by 252 mg $NaHCO_3$, 12.14 mg $NaNO_3$, 0.178 mg $NaH_2PO_4{\cdot}H_2O$, 2.21 mg NaF, 70.6 mg $NaSiO_3{\cdot}5H_2O$, 147 mg $CaCl_2{\cdot}2H_2O$ and 128.3 mg $MgSO_4{\cdot}7H_2O$ dissolution in 1 L of distilled water.

2.3. Arsenic adsorption on MgO

Batch adsorption experiments were carried in order to record the adsorption isotherms of MgO and evaluate its arsenic removal efficiency in the alkaline pH range. Around 20–25 mg of fine powder were dispersed in 200 mL of As(III) or As(V) solutions inside 300 mL conical flasks. The flasks were placed on an orbital shaker and stirred at 20 °C for 24 h. Initial As(III) and As(V) concentrations varied between 0.25 and 12.5 mg/L. The tests were performed at pH-values 10–12, since at lower pH values MgO is soluble in water. At the end of the experiments the suspensions were filtered through a 0.45 μm pore-size membrane and a drop of concentrated HNO_3 was added into the filtrate to preserve arsenic species. Residual arsenic concentration was determined using a Perkin Elmer AAnalyst 800 graphite furnace atomic absorption spectrophotometer.

The adsorption mechanism of As(III) and As(V) in aqueous solution (pH 11) onto MgO was investigated using X-ray absorption fine structure (XAFS) spectroscopy. The XAFS spectra were recorded at the C-beamline of the DORIS storage ring of the Synchrotron Radiation (SR) Facility HASYLAB. A double Si(1 1 1) crystal monochromator was employed and the spectra acquisition was done in the fluorescence yield mode using a 7-element Si-drift detector positioned on the horizontal plane at right angle to the SR beam. The Pt—L_{III} absorption edge (at 11,564 eV) of a thin Pt foil was used for the energy calibration. In order to achieve sufficient absorption intensity, MgO samples of 1 g/L were saturated with 75 mg/L either As(III) or As(V) solution in distilled water.

2.4. Adsorbent saturation and regeneration circuit

Most of the applied arsenic adsorbents appear to have a very low removal efficiency for As(III) compared to As(V), due to the

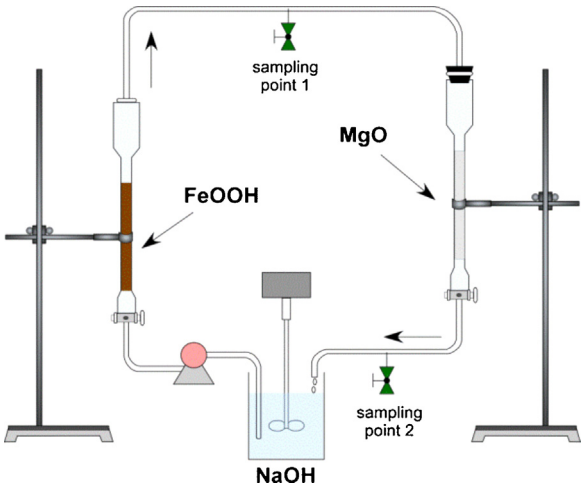

Fig. 1. Scheme of the laboratory on-site regeneration process using MgO.

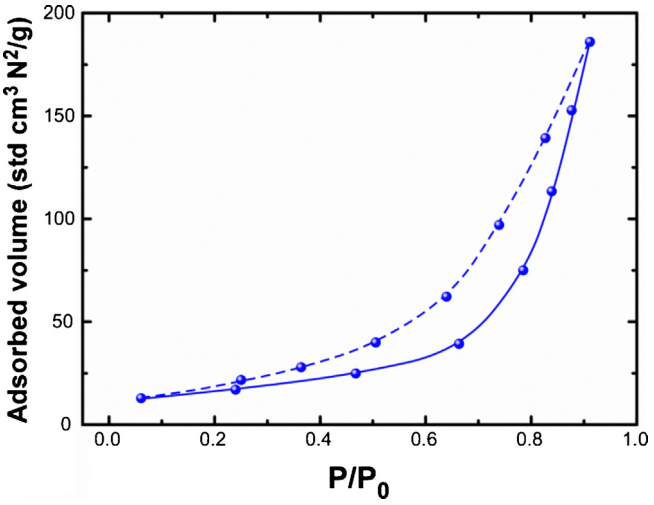

Fig. 2. Gas nitrogen adsorption (dotted line) and desorption (solid line) isotherms for MgO.

predomination of uncharged arsenite species (H_3AsO_3) at pH range encountered in natural waters [26,27]. In practice, when As(III) is present, a chemical or biological pre-oxidation step is embodied [28,29], followed by the removal of arsenic in the form of As(V). Therefore, the spent adsorbents of full scale treatment plants contain almost exclusively As(V), which in turn implies that the alkaline regeneration stream will contain only the leached As(V). For this reason, regeneration experiments were carried out using a column saturated with As(V).

For optimization of alkaline leaching procedure, 2 g of spent FeOOH samples containing 10 ± 0.2 mg As(V)/g were rotary stirred for 24 h with 25 mL NaOH solution in the concentration range between 0.01 and 0.1 M. Then, the FeOOH samples were filtered through a 0.45 μm membrane and their arsenic content was determined using a Perkin Elmer AAnalyst 800 graphite furnace atomic absorption spectrophotometer.

The efficiency of MgO as a medium to capture leached arsenic during the regeneration of a saturated adsorbent, was evaluated by monitoring the continuous recirculation of a NaOH solution between two columns containing the saturated iron oxy-hydroxide and MgO. At first, a glass column filled with 8 g of granular FeOOH (250–500 μm) was separately saturated by passing a 250 μg/L NSF water solution As(V) equilibrated at pH 7. This rapid small-scale column test (RSSCT) ran at a flow rate of 580 mL/h and employing an empty bed contact time (EBCT) of 1.2 min [30]. For the regeneration of this adsorbent the column was serially attached with an MgO column and a 0.05 N NaOH solution was recirculated at a flow rate set to 580 mL/h (Fig. 1). The MgO column contained 32 g of granular material operated at an EBCT of 5 min. The inner diameter of glass columns was 1.1 cm and 2 cm for iron oxy-hydroxide and MgO, respectively. Both columns had a height of 40 cm and they were equipped with PTFE valves, caps and glass frit in the bottom. In this setup, the NaOH stream ran up-flow through the FeOOH column and down-flow through the MgO column.

Samples were collected at regular intervals before (sampling point 1) and after (sampling point 2) the MgO column to monitor arsenic concentration. Eventually, regeneration process was completed in 24 h. NSF water was then passed through the FeOOH column at the same flow rate until the pH value reached 7.5. The success of the regeneration was verified by the measurement of residual arsenic content in FeOOH granules and the determination of arsenic removal efficiency of the regenerated material by repeating the RSSCT adsorption step.

2.5. Stabilization/Utilization of spent MgO

In order to propose an integrated and environmentally safe procedure for the disposal of the spent arsenic saturated MgO, the possibility of its use as an additive in building materials was investigated. Concrete cylindrical specimens were prepared by press-forming of mixtures containing cement, sand, dolomite and calcium stearate with water and the addition of spent MgO at 3 and 5 wt% of total mass in substitution of dolomite [31]. The details of the preparation parameters are summarized in Table 1. In order to prove the successful arsenic stabilization in concrete, leaching tests were performed according to the EN 12457 [32] and TCLP protocols [33]. Finally, the specimens were tested for compressive strength, according to European standard methods and procedures [34] to testify that MgO addition does not affect their applicability as building materials.

3. Results and discussion

3.1. Surface characterization

The nitrogen adsorption isotherms of MgO (Fig. 2) were classified of type IV, which is characteristic of the mesoporous materials, according to the Brunauer, Deming, Deming, Teller (BDDT) classification. The determination of surface morphological characteristics of the used MgO by the BET method showed a specific surface area of 59 m^2/g, a pore volume 0.14 mL/g and a mean pore diameter 156 Å. The large pore size of MgO allows arsenate ions to diffuse into the pore channel of the mesoporous material with relevant convenience, since their radius is significantly smaller ($H_2AsO_4^-$: 4.16 Å, $HAsO_4^{2-}$: 3.97 Å) [35] than the corresponding of MgO. Therefore, arsenic can potentially be initially adsorbed onto the surface of the MgO and when the exterior surface reached saturation it can enter into the pores and bind to the interior surfaces of the particles. The corresponding characteristics for the FeOOH were 155 m^2/g, 0.23 mL/g and 30 Å.

The isoelectric point of MgO was identified by plotting the zeta-potential curve at the pH range 9–14 (Fig. 3). The surface becomes practically neutral at approximately 12, while the value for the FeOOH adsorbent was 7.3. Such high IEP value indicates that an efficient arsenic adsorption can be maintained by MgO up to a solution pH of 12, which could be utilized for the refreshment of NaOH solutions commonly applied for adsorbents regeneration.

Table 1
Formula of the mixture and preparation parameters for the concrete specimens.

Ingredient	Spent MgO (wt%)			Preparation parameters	
	0	3	5		
Sand (0–1 mm) (g)	64	64	64	Water to cement ratio	0.35
Cement (g)	21	21	21	Pressure applied (kg/cm^2)	175
Dolomite (0–1 mm) (g)	14.5	11.5	9.5	Aging time (d)	43
Calcium stearate (g)	0.5	0.5	0.5	Specimens dimensions (cm)	Height: 22
Spent MgO (g)	0	3	5		Diameter: 1.7

3.2. Arsenic adsorption by MgO

Experimental data for As(V) adsorption are shown in Fig. 4a and were analyzed by fitting isotherm data to the Freundlich and Langmuir models. According to the Freundlich equation, the amount of arsenic adsorbed per unit mass of adsorbent, Q, is given by:

$$Q = K_F C_e^{1/n}$$

where C_e is the equilibrium arsenic concentration and K_F and n are constants related to adsorption capacity and intensity, respectively. The Langmuir equation has the following form:

$$Q_e = \frac{Q_{max} K_L C_e}{1 + K_L C_e}$$

where Q_e is the quantity of arsenic sorbed on the adsorbent for equilibrium concentration C_e, Q_{max} is the maximum arsenic adsorption capacity, K_L is the Langmuir constant.

The calculated fitting parameters for As(V) adsorption are summarized in Table 2, which indicate that Freundlich model describes better As(V) adsorption isotherms. In addition, Fig. 4a shows that the optimum pH for As(V) adsorption was 10, where a maximum adsorption capacity 59.4 mg As(V)/g was calculated (Table 2) for residual concentration near 5 mg/L. As the pH value increases close to the IEP (pH 12), the adsorption capacity of As(V) gradually decreases both due to the reduction of MgO positive surface charge and to the domination of the trivalent AsO_4^{3-} oxy-anion against the $HAsO_4^{2-}$ one [36]. It is also important to mention that the adsorption capacity of MgO at equilibrium concentration equal to the regulation limit for drinking water (10 μg/L) at the pH range 10–12 (Table 2) is similar to that of FeOOH determined at water pH values 6–8 [25].

On the contrary, As(III) adsorption (Fig. 4b) follows S-type isotherms indicating lower affinity and "cooperative adsorption". This type of isotherm implies an indefinite multi-layer formation, since after monolayer completion, adsorption continues by forming successive layers. In this case, the removal capacity is maximized at pH 11, where around 50 mg As(III)/g could be adsorbed for residual concentration 3 mg/L. However, the shape of the curve at pH 11 indicates that adsorption did not reach a plateau and consequently even higher maximum adsorption capacities can be achieved by further increasing the initial concentration of As(III). The significantly improved adsorption capacity at pH 11 could be attributed to the almost total dissociation of As(III) in monovalent $H_2AsO_3^-$. The lower adsorption capacity at pH 10 is due to the presence of uncharged H_3AsO_3, while the lower adsorption capacity at pH 12 could be attributed to bivalent $HAsO_3^{2-}$ domination against monovalent $H_2AsO_3^-$ [36]. The lowest residual As(III) concentration achieved in the examined pH range was estimated to be around 150 μg/L (Fig. 4b), which also indicates the weak affinity between As(III) and MgO.

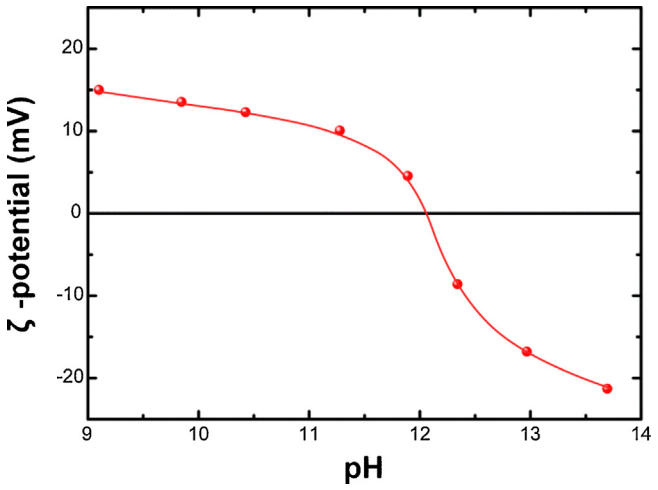

Fig. 3. Zeta-potential curve of MgO.

3.3. Adsorption mechanism

As previously mentioned, and also verified by column regeneration experiments of Section 3.4, the MgO reacts gradually with

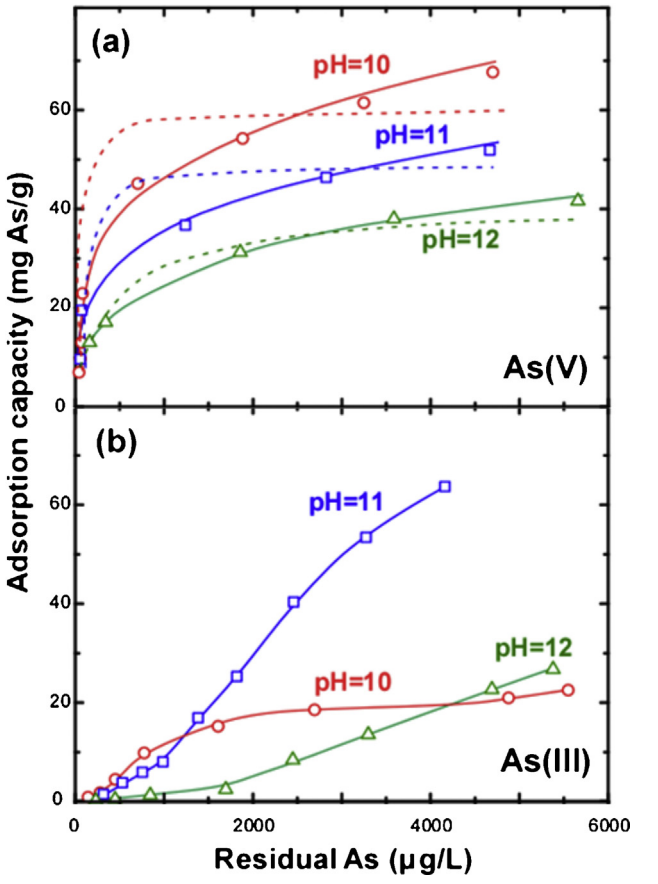

Fig. 4. Adsorption isotherms of MgO for As(V) (a) and As(III) (b) solutions in distilled water.

Table 2
Fitting parameters of Freundlich and Langmuir models used to simulate the As(V) adsorption isotherms of MgO.

pH	Freundlich				Langmuir		
	K_F ($(\mu g_{As}/mg_{ads})/(\mu g/L)^{1/\eta}$)	$1/\eta$	Q_{10}[a] ($\mu g_{As}/mg_{ads}$)	R^2	K_L ($L/\mu g_{As}$)	Q_{max} ($\mu g_{As}/mg_{ads}$)	R^2
As(V)							
10	9.1	0.240	15.4	0.994	21.9×10^{-3}	59.4	0.917
11	7.1	0.248	11.3	0.991	16.9×10^{-3}	46.8	0.897
12	2.8	0.317	5.5	0.994	2.2×10^{-3}	43.3	0.953

[a] Adsorption capacity at equilibrium concentration 10 μg/L.

water to form $Mg(OH)_2$, which in turn covers the surface of MgO grains. Therefore, As—K-edge EXAFS spectra, which are shown in Fig. 5, are most likely to signify As(V) and As(III) adsorption by $Mg(OH)_2$. The energy position of the characteristic "white line" in the XANES spectra is representative of the As valance state (Fig. 6). For As(III) it appears red-shifted by approximately 3.5 eV compared to the corresponding position for As(V) [37]. The "white line" in the studied samples appears at the expected energy position, indicating that no oxidation of As(III) to As(V) took place during the adsorption process.

The arsenic species adsorption was studied by As—K-edge EXAFS. The $\chi(k)$ spectra, obtained after subtraction of the atomic background and transformation from the energy space to the k-space, were fitted using various models. The analysis of the EXAFS spectra was performed using the FEFF package [38]. The $\chi(k)$ spectra and the corresponding Fourier transforms (FT) are shown in Fig. 5, along with the fitting curves obtained using the optimum model. The FT of the As(III) adsorbed onto $Mg(OH)_2$ exhibits an intense double peak at around 3 Å, which precludes outer or inner sphere complex formation by adsorbed arsenite complexes. On the contrary, it is most likely to be attributed to the agglomeration of As(III) species and more specifically to the formation of AsO_3 polymer chains, as indicated in Fig. 5c. Such layered/chain structures are formed in As oxides like claudetite which is an As_2O_3 polytype [39]. On the other hand, in the case of As(V) adsorption a low-intensity peak appears in the FT at approximately 3 Å. In this case a model of arsenate forming monodentate complexes with the surface of $Mg(OH)_2$ was used.

The fitting results listed in Table 3 indicate the different bonding geometry of As(III) and As(V). More specifically, the As—O distance in the former case is significantly higher [40], verifying that adsorption does not cause variation of the oxidation state of As, as it is also observed with XANES spectroscopy. Furthermore, in the case of As(III) adsorption, the As atom binds with three oxygen atoms at the distance of 1.77 Å that is typical for As(III) oxocomplexes which, in the case of pH value equal to 11, is more stable as $H_2AsO_3^-$ [36]. Regarding the 2nd and 3rd nearest neighboring shells, the detection

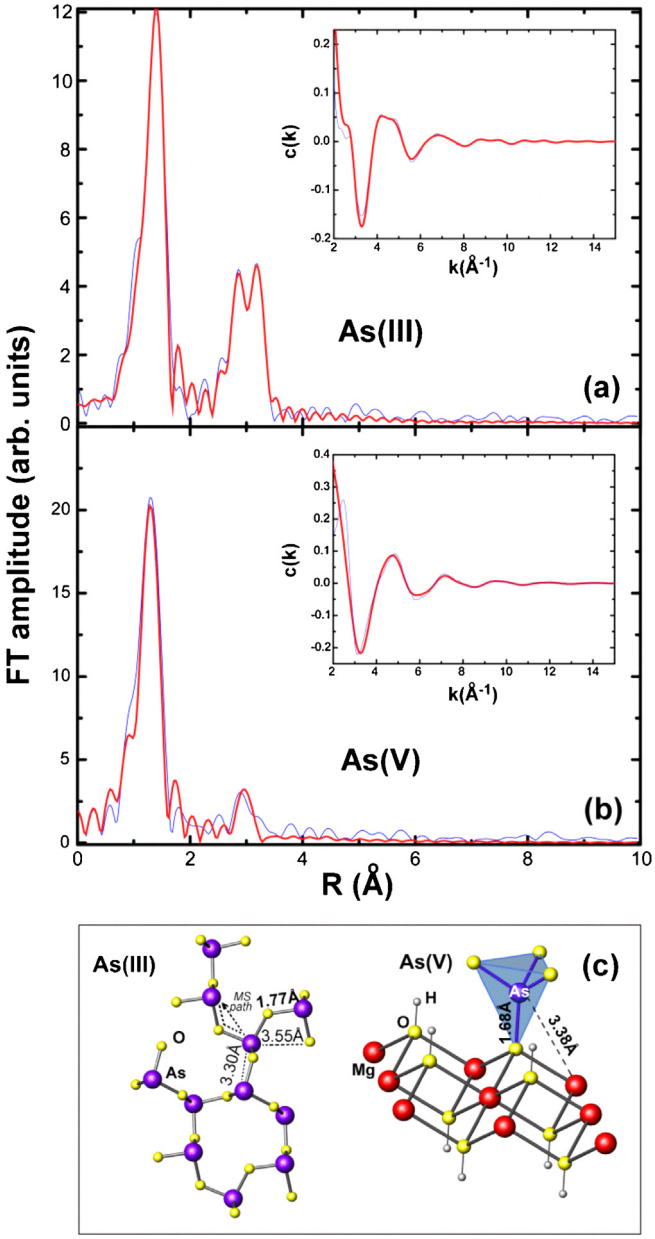

Fig. 5. Fourier transform amplitude of the k^3 weighted $\chi(k)$ As—K-edge EXAFS spectra of As(III) (a) and As(V) (b) adsorption onto $Mg(OH)_2$. The corresponding $\chi(k)$ spectra are shown in the inset. Thin and thick solid lines correspond to the experimental and the fitting curves, respectively. (c) Structural models for the arsenite polymers and arsenate monodentate absorption onto $Mg(OH)_2$ surface.

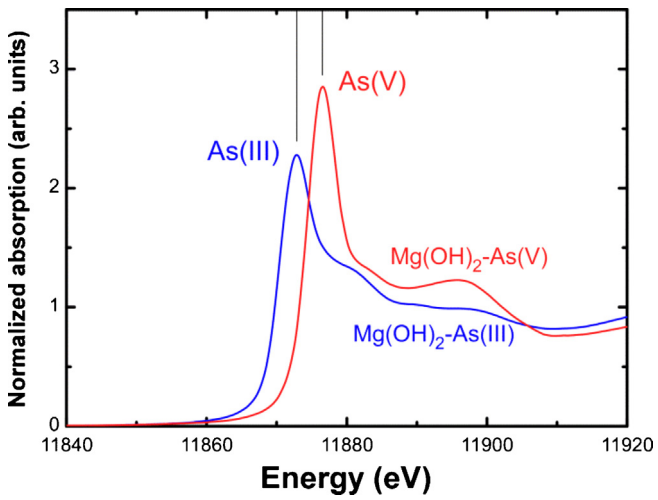

Fig. 6. As—K-edge XANES spectra of As(III) and As(V) adsorption. Vertical lines indicate the position of "white lines" that correspond to the two oxidation states of As.

Table 3
Fitting results of the As—K-edge EXAFS spectra of the As(III) and As(V) adsorption. The spectra of As(III) and As(V) were fitted using arsenite polymer chains and monodentate complexes forming inner sphere complexes onto $Mg(OH)_2$, respectively. In the former case, the use of an As—O—As multiple scattering (MS) path improved the fitting quality. *N* is the coordination number, σ^2 is the Debye–Waller factor and *R* the nearest neighbor distance. The quoted errors correspond to the uncertainty of the fitting.

	As(III)			As(V)		
	R (Å)	*N*	$\sigma^2 \times 10^{-3}$(Å^2)	*R* (Å)	*N*	$\sigma^2 \times 10^{-3}$(Å^2)
As—O	1.77 ± 0.01	3.0 ± 0.1	4.0 ± 0.4	1.68 ± 0.01	4.1 ± 0.4	2.4 ± 0.4
As—As	3.30 ± 0.01	2.2 ± 0.8	4.9 ± 1.7	–	–	–
As—Mg	–	–	–	3.38 ± 0.02	2.1 ± 0.4	4.0 ± 0.7
As—O	3.55 ± 0.02	5.7 ± 0.9	4.7 ± 2.5	–	–	–
As—O—As (MS)	3.42	2	4.9	–	–	–

of As and O neighbors, respectively, at distances similar to those observed in layered As_2O_3 structures, indicates that As(III) forms layers and/or chains of AsO_3 pyramids which are weakly adsorbed onto $Mg(OH)_2$ surface. However, the formation of As_2O_3 multilayers could not be excluded. Multilayer adsorption of As(III) on the surface of $Mg(OH)_2$ is also concluded from the S-type isotherms.

Fig. 5b indicates that As(V), which in pH 11 is found as $HAsO_4^{2-}$, is coordinated with 4 oxygen atoms at the distance of 1.68 Å which is consistent with the oxidation state of As(V) [41]. The small contribution at the distance of 3.38 Å corresponds to Mg atoms and could be attributed to the formation of monodentate inner sphere complexes absorbed on the $Mg(OH)_2$ (brucite) surfaces as shown in Fig. 5c, which verify the strong As(V) adsorption.

3.4. Regeneration of FeOOH using MgO

Preliminary experiments showed that the optimal As(V) leachability was obtained by a 0.05 N NaOH solution, which resulted a pH range 11–11.5 (Fig. 7). At higher pH values, extended leachability of the bound arsenic was performed, which, however, was accompanied by FeOOH disintegration leading to a major reduction of its mechanical strength that is required for reuse. On the contrary, arsenic leachability was significantly decreased at lower NaOH concentrations, implying both longer regeneration time and lower efficiency.

Considering the MgO column, an EBCT of at least 3 min was required for efficient (>90%) As(V) capture, especially at the beginning of the procedure when high As(V) concentrations were leached (Fig. 8). However, to comply with the two step adsorption process, which includes the MgO hydrolysis and As(V) adsorption onto $Mg(OH)_2$, a contact time of 5 min was applied. The MgO hydrolysis to $Mg(OH)_2$ during regeneration procedure is signified

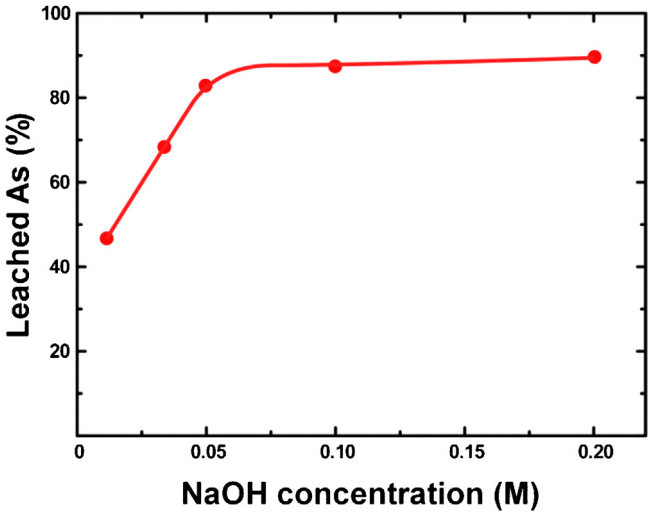

Fig. 7. Arsenic leached from FeOOH as a function of NaOH concentration.

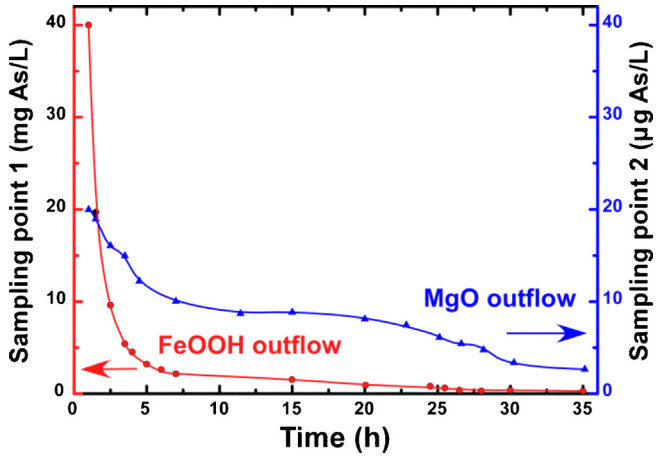

Fig. 8. Arsenic concentration monitoring at the outflow of saturated FeOOH and MgO columns. Note the different concentration units in the two axes.

by the strong endothermic peak at around 420 °C in the heat flow curve (Fig. 9) [42], while weight loss curve indicates that more than 60 wt% of MgO was hydrolyzed to $Mg(OH)_2$. XRD diagrams of Fig. 10 also support the extended MgO hydration and formation of $Mg(OH)_2$ during contact period. It should be pointed that such structural and compositional change occurs following a mechanism consisting of (i) water adsorption and diffusion, (ii) MgO dissolution and (iii) supersaturation, nucleation and growth of $Mg(OH)_2$ [23]. The precipitation of $Mg(OH)_2$ affects the observed morphology of the material as shown by the sharpening and homogenization of granules size after the regeneration cycle (Fig. 11). The hydroxylation of material's surface results in the predomination of $MgOH^+$ sites at the pH range 11–12 which explains improved adsorption efficiency.

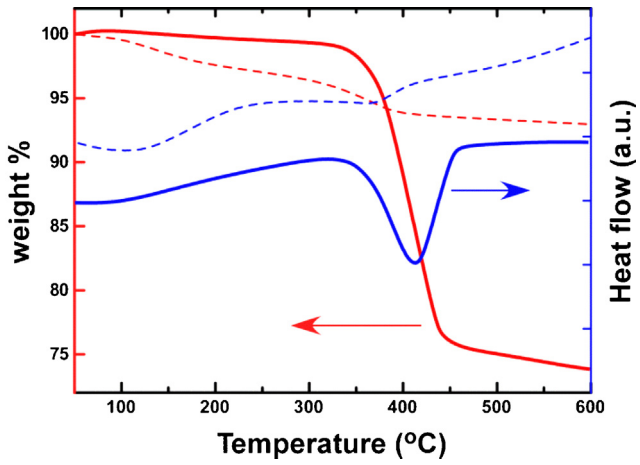

Fig. 9. Thermal curves of raw MgO (dotted lines) and spent MgO (solid lines).

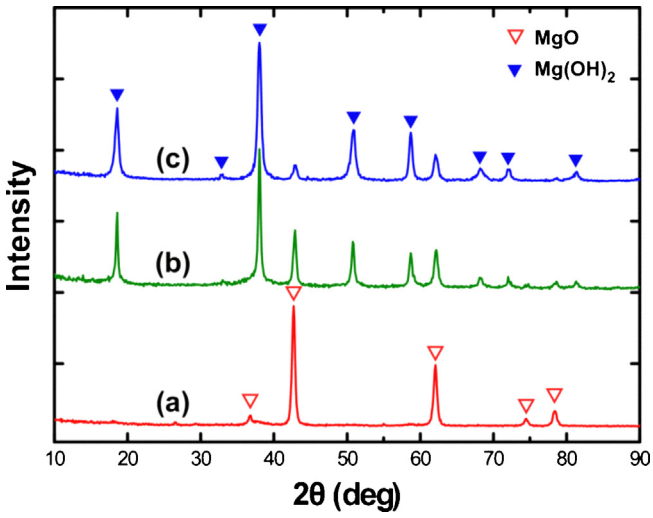

Fig. 10. XRD diagrams of raw MgO (a), material received after a 24 h batch adsorption test at pH 11 (b) and spent material after regeneration process (c).

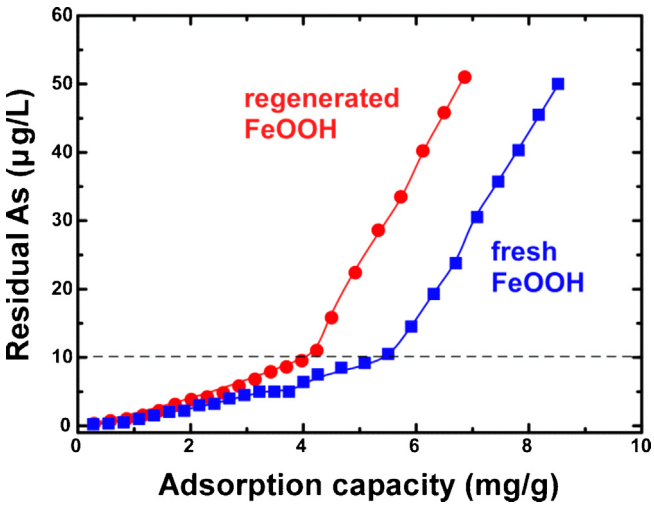

Fig. 12. Breakthrough curves of As(V) adsorption by the fresh and regenerated FeOOH (NSF water at pH 7).

Fig. 8 demonstrates the effluent arsenic concentrations of saturated FeOOH and MgO column during regeneration process. It is concluded that the major part of the adsorbed arsenic from the FeOOH column is leached within the first 7 h. The success of the regeneration process was confirmed by the remaining arsenic percentage in FeOOH granules, which decreased by almost 90% (from 8.5 to 0.9 mg As/g). Furthermore, the low arsenic concentration (<25 μg/L) at MgO column effluent indicates that leached arsenic is captured by MgO. Another important observation is that at the end of regeneration process, the equilibrium arsenic concentration in NaOH solution was practically zero (<10 μg/L), and therefore NaOH solution could be recycled in the next regeneration cycle.

The regenerated FeOOH column was reused for As(V) removal under the same RSSCT experiment. Breakthrough curves of FeOOH column before and after the regeneration process (Fig. 12), showed that the adsorption capacity decreased by almost 20%. More specifically, the Q_{10} adsorption capacity 5.7 mg As/g of the fresh FeOOH, was decreased to 4.4 mg As(V)/g after regeneration. This efficiency loss should be mainly attributed to the remaining arsenic content (0.9 mg As/g), as well as to the interfering parameters such as phosphates, originating from the test water (NSF) used for the adsorbents saturation, which strongly bound onto FeOOH.

To clarify the magnitude of cost saving by using MgO for FeOOH regeneration it should be mentioned that the cost of commercial

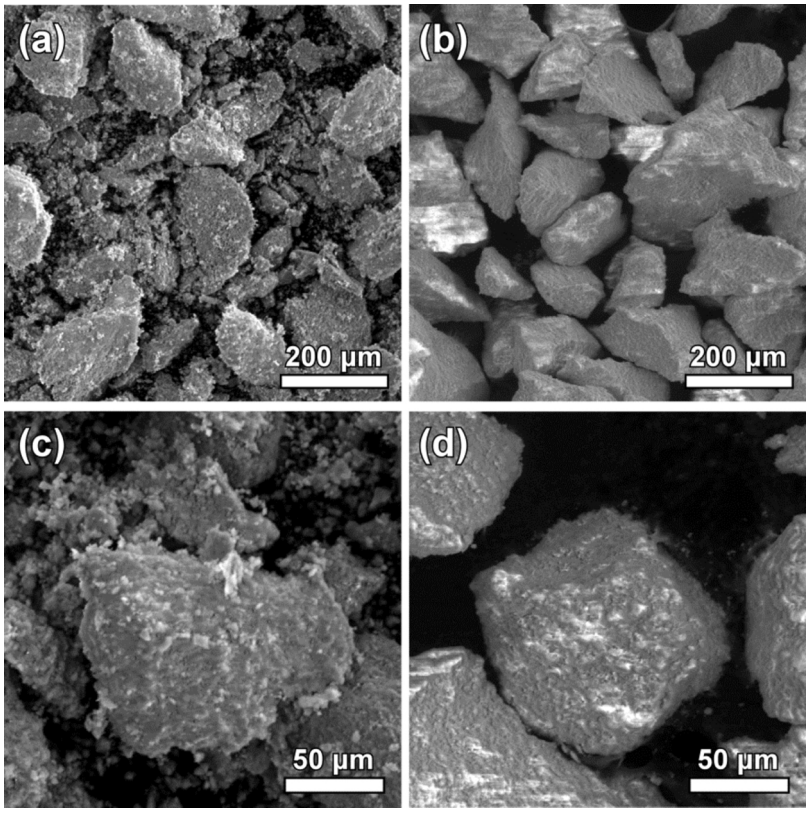

Fig. 11. SEM images of raw MgO (a) and spent material after regeneration process (b). Corresponding high magnification images (c, d).

Table 4
MOR values and leaching tests results of concrete specimens prepared with addition of saturated $MgO/Mg(OH)_2$.

	Spent $MgO/Mg(OH)_2$ (wt%)		
	0	3	5
MOR (kgf/cm^2)	1.9	1.8	1.2
EN 12457-01[a] (mg/kg)	<0.01	<0.01	<0.01
TCLP[b] (μg/L)	<1	<1	<1

[a] Limit for inert wastes 0.5 mg/kg.
[b] Limit for non-hazardous wastes 5×10^3 μg/L.

FeOOH is around 100 times higher than the respective for MgO. According to adsorption isotherms, the expected maximum treatment capability of MgO is expected to support at least 5 cycles of regeneration at breakthrough concentration of 10 μg/L in the washing stream. Therefore, taking into account the installation and operational expenses for the regeneration process as well as the small reduction of regenerated FeOOH efficiency, the cost of arsenic removal decreases by at least 75% when the proposed process is applied.

3.5. Saturated $MgO/Mg(OH)_2$ disposal

Clinker, which is the main component of cement, always contains a small amount of MgO. Studies have shown that a MgO content below 3 wt% is beneficial to the clinker and to the relevant concrete building materials properties, whereas when MgO content significantly exceeds 3 wt% the mechanical strength of the concrete definitively decreases [43]. For this reason, a MgO percentage 0–5 wt% in the $MgO/Mg(OH)_2$ commercial concrete products was established. In order to examine the possibility of utilizing the arsenic-saturated $MgO/Mg(OH)_2$ as an additive in building materials, the mechanical and leaching properties of concrete specimens prepared by 3 and 5 wt% addition were investigated.

The modulus of rupture (MOR) values and the leaching tests results, determined for the concrete specimens prepared by the addition of spent MgO in substitution of dolomite, are summarized in Table 4. The results show an extremely low leachability of arsenic. This should apparently be attributed to the fixation through chemical bonds of the $MgO/Mg(OH)_2$ grains in the concrete solid matrix, resulting in turn in arsenic immobilization. Furthermore, the results of Table 4 indicate that the addition of up to 3 wt% did not substantially affect the mechanical strength of the concrete specimens, as the value of MOR decreased by only 5%. However, the addition of 5 wt% resulted in the reduction of MOR by 40%. These observations are in agreement with the mentioned analysis for the effect of MgO addition in concrete products. In conclusion, it appears that the incorporation of spent $MgO/Mg(OH)_2$ in commercially concrete products is possible, since leaching test results meet the limits for inert waste disposal without affecting their mechanical strength.

4. Conclusions

The possibility of MgO application as a regenerating medium for arsenic adsorbents was verified by both batch adsorption tests and column tests simulating a realistic recirculation configuration. On this direction, the main advantage of MgO relies with its improved affinity with arsenic species localized at strong alkaline environments. As observed, MgO can adsorb high quantities of arsenic at the pH range 10–12 at batch experiment as well as by a flowing NaOH stream and practically eliminate residual concentrations in the outflow. The proposed mechanism of arsenic adsorption on MgO includes its hydrolysis and the chemisorption, in the case of As(V), onto $Mg(OH)_2$. The monitoring of a dynamic continuous flow recirculation setup in which arsenic is leached by NaOH from an iron oxy-hydroxide containing column and adsorbed by granulated MgO in another column revealed that the adsorbent regeneration results in around 80% recovery of its initial removal efficiency. The spent $MgO/Mg(OH)_2$ from such process was found to be compatible as a substitute for building materials according to the leaching and mechanical strength tests.

Acknowledgments

This work was supported by the European Commission FP7/Research for SMEs "AquAsZero", project no: 232241. Part of this work was implemented within the framework of Action "Supporting Postdoctoral Researchers" of Operational Program Education and Lifelong Learning (Action's Beneficiary: GSRT), and is co-financed by ESF and Greek State. The XAFS measurements were financially supported by DESY and the European Community's Seventh Framework Program (FP7/2007–2013) under grant agreement no: 312284.

References

[1] C.K. Jain, I. Ali, Arsenic: occurrence, toxicity and speciation techniques, Water Res. 34 (2000) 4304–4312.
[2] I. Celik, L. Gallicchio, K. Boyd, T.K. Lamc, G. Matanoski, X. Tao, M. Shiels, E. Hammond, L. Chen, K.A. Robinson, L.E. Caulfield, J.G. Herman, E. Guallar, A.J. Alberg, Arsenic in drinking water and lung cancer: a systematic review, Environ. Res. 108 (2008) 48–55.
[3] M.G. Mitrakas, P.C. Panteliadis, V.Z. Keramidas, R.D. Tzimou-Tsitouridou, C.A. Sikalidis, Predicting Fe^{3+} dose for As(V) removal at pHs and temperatures commonly encountered in natural waters, Chem. Eng. J. 155 (2009) 716–721.
[4] T.F. Lin, J.K. Wu, Adsorption of arsenite and arsenate within activated alumina grains: equilibrium and kinetics, Water Res. 35 (2001) 2049–2057.
[5] L. Wang, A. Chen, K. Fields, Arsenic removal from drinking water by ion exchange and activated alumina plant, EPA-600/R00-/088, U.S. EPA, 2000.
[6] W. Chen, R. Parette, J. Zou, F.S. Cannon, B.A. Dempsey, Arsenic removal by iron-modified activated carbon, Water Res. 41 (2007) 1851–1858.
[7] K. Banerjee, G.L. Amy, M. Prevost, S. Nour, M. Jekel, P.M. Gallagher, C.D. Blumenscheine, Kinetic and thermodynamic aspects of adsorption of arsenic onto granular ferric hydroxide (GFH), Water Res. 42 (2008) 3371–3378.
[8] X.H. Guan, J. Wang, C.C. Chusuei, Removal of arsenic from water using granular ferric hydroxide: macroscopic and microscopic studies, J. Hazard. Mater. 156 (2008) 178–185.
[9] S. Bang, M. Patel, L. Lippincott, X. Meng, Removal of arsenic from groundwater by granular titanium dioxide adsorbent, Chemosphere 60 (2005) 389–397.
[10] X. Guana, J. Du, X. Meng, Y. Sun, B. Sun, Q. Hu, Application of titanium dioxide in arsenic removal from water: a review, J. Hazard. Mater. 215-216 (2012) 1–16.
[11] J. Guo, X. Cai, Y. Li, R. Zhai, S. Zhou, P. Na, The preparation and characterization of a three-dimensional titanium dioxide nanostructure with high surface hydroxyl group density and high performance in water treatment, Chem. Eng. J. 221 (2013) 342–352.
[12] R. Li, Q. Li, S. Gao, J.K. Shang, Exceptional arsenic adsorption performance of hydrous cerium oxide nanoparticles. Part A. Adsorption capacity and mechanism, Chem. Eng. J. 185–186 (2012) 127–135.
[13] W. Xu, J. Wang, L. Wang, G. Sheng, J. Liu, H. Yu, X.-J. Huang, Enhanced arsenic removal from water by hierarchically porous CeO_2–ZrO_2 nanospheres: role of surface- and structure-dependent properties, J. Hazard. Mater. 260 (2013) 498–507.
[14] S. Tresintsi, K. Simeonidis, S. Estradé, C. Martinez-Boubeta, G. Vourlias, F. Pinakidou, M. Katsikini, E.C. Paloura, G. Stavropoulos, M. Mitrakas, Tetravalent manganese feroxyhyte: a novel nanoadsorbent equally selective for As(III) and As(V) removal from drinking water, Environ. Sci. Technol. 47 (2013) 9699–9705.
[15] L. Wang, W.E. Condit, A.S.C. Chen, Technology selection and system design U.S.EPA arsenic removal technology demonstration program round 1, EPA/600/R-05/001, U.S. EPA, 2004.
[16] C. Jing, S. Liu, M. Patel, X. Meng, Arsenic leachability in water treatment adsorbents, Environ. Sci. Technol. 39 (2005) 5481–5487.
[17] S. Tresintsi, K. Simeonidis, A. Zouboulis, M. Mitrakas, Comparative study of As(V) removal by ferric coagulation and oxy-hydroxides adsorption: Laboratory and full scale case studies, Desalin. Water Treat. 51 (2013) 2872–2880.
[18] D. Mohan, C.U. Pittman Jr., Arsenic removal from water/wastewater using adsorbents – a critical review, J. Hazard. Mater. 142 (2007) 1–53.
[19] B.R. Manna, S. Dey, S. Debnath, U.C. Ghosh, Removal of arsenic from groundwater using crystalline hydrous ferric oxide (CHFO), Water Qual. Res. J. Can. 38 (2003) 193–210.
[20] Y. Liu, Q. Li, S. Gao, J.K. Shangz, Exceptional As(III) sorption capacity by highly porous magnesium oxide nanoflakes made from hydrothermal synthesis, J. Am. Chem. Soc. 94 (2011) 217–223.

[21] X.Y. Yu, T. Luo, Y. Jia, Y.X. Zhang, J.H. Liu, X.J. Huang, Porous hierarchically micro/nanostructured MgO: morphology control and their excellent performance in As(III) and As(V) removal, J. Phys. Chem. C 115 (2011) 22242–22250.
[22] Y. Jia, T. Luo, X.-Y. Yu, B. Sun, J.-H. Liu, X.-J. Huang, A facile template free solution approach for the synthesis of dypingite nanowires and subsequent decomposition to nanoporous MgO nanowires with excellent arsenate adsorption properties, RSC Adv. 3 (2013) 5430–5437.
[23] S.D.F. Rocha, M.B. Mansur, V.S.T. Ciminelli, Kinetics and mechanistic analysis of caustic magnesia hydration, J. Chem. Technol. Biotechnol. 79 (2004) 816–821.
[24] S. Ardizzone, C.L. Bianchi, B. Vercelli, MgO powders: interplay between adsorbed species and localisation of basic sites, Appl. Surf. Sci. 126 (1998) 169–175.
[25] S. Tresintsi, K. Simeonidis, G. Vourlias, G. Stavropoulos, M. Mitrakas, Kilogram-scale synthesis of iron oxy-hydroxides with improved arsenic removal capacity: study of Fe(II) oxidation–precipitation parameters, Water Res. 46 (2012) 5255–5267.
[26] P. Lakshmipathiraj, B.R.V. Narasimhan, S. Prabhakar, G.B. Raju, Adsorption of arsenate on synthetic goethite from aqueous solutions, J. Hazard. Mater. B 136 (2006) 281–287.
[27] X. Guan, J. Du, X. Meng, Y. Sun, B. Sun, Q. Hu, Application of titanium dioxide in arsenic removal from water: a review, J. Hazard. Mater. 215-216 (2012) 1–16.
[28] S. Sorlini, F. Gialdini, Conventional oxidation treatments for the removal of arsenic with chlorine dioxide, hypochlorite, potassium permanganate and monochloramine, Water Res. 44 (2010) 5653–5659.
[29] I. Katsoyiannis, A. Zouboulis, H. Althoff, H. Bartel, As(III) removal from groundwater using fixed-bed up-flow bioreactors, Chemosphere 47 (2002) 325–332.
[30] P. Westerhoff, D. Highfield, M. Badruzzaman, Y. Yoon, Rapid small-scale column tests for arsenate removal in iron oxide packed bed columns, J. Environ. Eng. 131 (2005) 262–271.
[31] C. Sikalidis, M. Mitrakas, Utilization of electric arc furnace dust as raw material for the production of ceramic and concrete building products, J. Environ. Sci. Health Part A – Toxic/Hazard. Subst. Environ. Eng. 41 (2006) 1943–1954.
[32] European Standard EN12457-1/2002, Characterisation of waste–leaching–compliance test for leaching of granular waste materials and sludges. Part 1, 2002.
[33] U.S. EPA, Method 1311. Toxicity Characteristic Leaching Procedure (TCLP). Test Methods for Evaluating Solid Waste, Physical/Chemical Methods (SW-846), third ed., 1992.
[34] European Standard Methods of Test for Masonry Units, CEN, European Committee for Standardization, Determination of Compressive Strength EN 772-01, 2000.
[35] Y. Kim, Ch. Kim, I. Choi, S. Rengaraj, J. Yi, Arsenic removal using mesoporous alumina prepared via a templating method, Environ. Sci. Technol. 38 (2004) 924–931.
[36] M. Streat, K. Hellgardt, N.L.R. Newton, Hydrous ferric oxide as an adsorbent in water treatment. Part 2. Adsorption studies, Process Safety Environ. Protect. 86 (2008) 11–20.
[37] P. Kappen, J. Webb, An EXAFS study of arsenic bonding on amorphous aluminium hydroxide, Appl. Geochem. 31 (2013) 79–83.
[38] A.L. Ankudinov, B. Ravel, J.J. Rehr, S.D. Conradson, Real-space multiple-scattering calculation and interpretation of X-ray-absorption near-edge structure, Phys. Rev. B 58 (1998) 7565–7576.
[39] A.J. Frueh Jr., The crystal structure of claudetite (monoclinic As_2O_3), Am. Mineral. 36 (1951) 833–850.
[40] M. Pena, X. Meng, G.P. Korfiatis, Ch. Jing, Adsorption mechanism of arsenic on nanocrystalline titanium dioxide, Environ. Sci. Technol. 40 (2006) 1257–1262.
[41] D.A. Polya, A.G. Gault, R.A. Wogelius, E.X.A.F.S. Direct, evidence for incorporation of As^{5+} in the tetrahedral site of natural andraditic garnet, Am. Mineral. 92 (2007) 1856–1861.
[42] F. Meshkani, M. Rezaei, Effect of process parameters on the synthesis of nanocrystalline magnesium oxide with high surface area and plate-like shape by surfactant assisted precipitation method, Powder Technol. 199 (2010) 144–148.
[43] X. Liu, Y. Li, Effect of MgO on the composition and properties of alite–sulphoaluminate cement, Cement Concrete Res. 35 (2005) 1685–1687.